Unbalanced-Mode Spiral Antenna Backed by an Extremely Shallow Cavity

OYANAGI, Hiroshi / YAMAUCHI, Junji / IGARASHI, Tatsuya / IITSUKA, Yasushi / NAKANO, Hisamatsu

(出版者 / Publisher)
IEEE

(雑誌名 / Journal or Publication Title)
IEEE Transactions on Antennas and Propagation / IEEE Transactions on Antennas and Propagation

(号 / Number)
6

(開始ページ / Start Page)
1625

(終了ページ / End Page)
1633

(発行年 / Year)
2009-06

Unbalanced-Mode Spiral Antenna Backed by an Extremely Shallow Cavity

Hisamatsu Nakano, *Fellow, IEEE*, Tatsuya Igarashi, Hiroshi Oyanagi, Yasushi Iitsuka, *Member, IEEE*, and Junji Yamauchi, *Senior Member, IEEE*

***Abstract*—This paper describes a two-arm Archimedean spiral antenna backed by a conducting cavity, where only one arm is directly excited, with the other arm being parasitically excited; in other words, the spiral arms are excited in an unbalanced mode. A balun circuit required for a conventional two-arm spiral is not used for this unbalanced-mode spiral. The design of the unbalanced-mode spiral is performed over a frequency range of $f_{\mathrm{Ld}} = 3$ GHz to $f_{\mathrm{Hd}} = 9$ GHz (1:3 bandwidth), where the antenna height is selected to be extremely small ($7\ \mathrm{mm} = 0.07$ wavelength at f_{Ld}) to realize a low-profile antenna. For reference, a corresponding spiral antenna excited in balanced mode is also analyzed. It is found that the unbalanced-mode spiral shows an acceptably small VSWR over the design frequency range of f_{Ld} to f_{Hd}. The radiation is circularly polarized around the antenna axis normal to the spiral plane. The gain shows behavior similar to that of the balanced-mode spiral. Results for other antenna heights (5 mm, 10.5 mm, and 14 mm) are also presented and briefly discussed. It can be said that the unbalanced-mode spiral is a circularly polarized wideband antenna with a simple feed system.**

***Index Terms*—Circular polarization, current decomposition, low-profile antenna, spiral antenna, unbalanced mode.**

I. Introduction

THE Archimedean spiral (ARCS) antenna is known for its wideband radiation characteristics [1]. In most cases, the number of arms is chosen to be two, and these two arms are excited in balanced mode (i.e., the same amplitude and a 180-degree phase difference between the two arms). Such a two-arm ARCS, referred to as a balanced-mode spiral (abbreviated as BALS), radiates a circularly polarized (CP) wave in the direction normal to the antenna plane. The CP radiation from the BALS has been qualitatively explained by using current-band theory [1] and quantitatively evaluated using the method of moments [2]–[4].

The BALS is excited using a coaxial line with a balun circuit, which transforms the unbalanced mode of the coaxial line into the balanced mode required for the BALS, performing impedance matching between the coaxial line and the BALS over a wide frequency range. Designing and installing such a wideband balun circuit [5], [6] for the two-arm spiral requires laborious efforts. This leads to the question of whether an ARCS antenna could be exited only with a coaxial line (no balun circuit), while still maintaining wideband radiation characteristics comparable to those of a corresponding BALS.

This paper presents an answer to the above question by designing a low-profile, cavity-backed, wideband, two-arm ARCS antenna excited without a balun circuit, where one arm is fed by a coaxial line and the other arm behaves as a parasitic element. This antenna is referred to as an unbalanced-mode Archimedean spiral antenna (abbreviated as UnBALS). So far, we have analyzed an UnBALS having an antenna height of one-quarter wavelength and revealed that the frequency bandwidth for the axial ratio is relatively wide (18%) [7]. In this paper, a low-profile UnBALS (0.07 wavelength antenna height) is investigated to obtain extremely wideband frequency characteristics (100%) for the axial ratio, input impedance, radiation pattern, and gain.

Five sections, including this introduction, constitute this paper. Section II describes the configuration of an UnBALS backed by a conducting cavity. For reducing the reflected currents from the arm ends of the UnBALS, a ring-shaped absorbing material [8]–[10] is applied to the cavity. The height of the antenna/cavity is chosen to be extremely small to realize a low-profile antenna that operates within a 100% design frequency bandwidth [from 3 GHz ($\equiv f_{\mathrm{Ld}}$) to 9 GHz ($\equiv f_{\mathrm{Hd}}$)]; a test height of 7 mm, corresponding to 0.07 wavelength at the lowest design frequency f_{Ld}, is chosen.

Section III presents the antenna characteristics of the UnBALS, over a frequency range from 2 GHz ($\equiv f_{\mathrm{La}} = f_{\mathrm{Ld}} - 1$) to 10 GHz ($\equiv f_{\mathrm{Ha}} = f_{\mathrm{Hd}} + 1$), together with the characteristics of a corresponding BALS. This section is composed of three subsections, A, B, and C, which describe the input impedance, radiation pattern, axial ratio, and gain characteristics as a function of frequency. These characteristics are calculated on the basis of the electric and magnetic fields obtained using the finite-difference time-domain method (FDTDM) [11], [12].

Section III-A discusses the input impedances of the UnBALS and BALS antennas, and Section III-B gives a comparison of the radiation patterns for these antennas. Subsequently, the asymmetry found in the radiation pattern with respect to the antenna axis (normal to the antenna plane) is explained, focusing on the currents along the two arms of the UnBALS. Each of these currents is decomposed into odd-mode and even-mode currents. Section III-C presents the frequency response of the axial ratio of the UnBALS, together with that of the BALS, within the analysis frequency range of f_{La} (2 GHz) to f_{Ha} (10 GHz). A comparison of the gains between the UnBALS and BALS is also made in Section III-C. Note that the theoretical results are verified with experimental results.

Manuscript received August 06, 2008; revised January 23, 2009. Current version published June 03, 2009.

The authors are with the College of Engineering, Hosei University, Koganei, Tokyo 184-8584, Japan (e-mail: nakano@hosei.ac.jp).

Color versions of one or more of the figures in this paper are available online at http://ieeexplore.ieee.org.

Digital Object Identifier 10.1109/TAP.2009.2019916

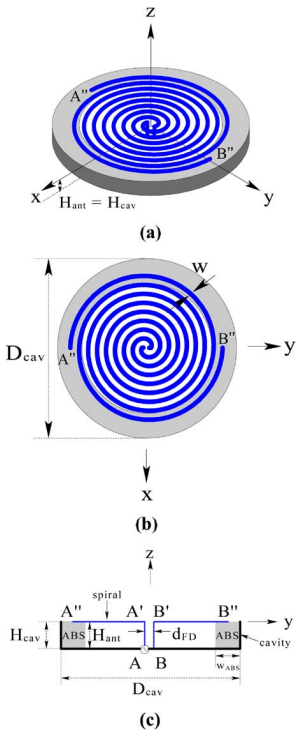

Fig. 1. Unbalanced-mode spiral (UnBALS). (a) Perspective view, (b) top view, and (c) side view.

Section IV presents supplemental data for gaining a better understanding of the UnBALS backed by a cavity discussed in Section III. The absorber attached to the cavity, the distance between the spiral plane and the bottom of the cavity (antenna height), and the feed line for the spiral are discussed. Finally, Section V summarizes the results obtained in this research.

II. Configuration

Fig. 1 shows an unbalanced-mode Archimedean spiral antenna (UnBALS) composed of two strip arms. The center line of the strip is defined by the Archimedean function $r = \mathrm{a_{sp}}\phi_{\mathrm{w}}$, where $\mathrm{a_{sp}}$ is the spiral constant and ϕ_{w} is the winding angle, ranging from the starting angle ϕ_{st} to the ending angle ϕ_{end}. The strip arm width is w and the antenna height is H_{ant}. The spiral arms are backed by a conducting cavity, whose diameter is D_{cav}. The height of the cavity (H_{cav}) is chosen to be the same as the antenna height: $H_{\mathrm{cav}} = H_{\mathrm{ant}}$. One of the arms is connected to the inner conductor of a coaxial feed line, while the other arm is short-circuited to the bottom of the cavity, as shown in Fig. 1(c), where the spacing between the two vertical arms (strip width w) is d_{FD}. Note that if both arms are excited with the same amplitude and a 180-degree phase difference, as shown in Fig. 2 (side view only), the spiral is designated as a balanced-mode spiral (BALS). The BALS has the same configuration as the UnBALS, except for the excitation.

We design an UnBALS that operates over a frequency range of $f_{\mathrm{Ld}} = 3$ GHz to $f_{\mathrm{Hd}} = 9$ GHz (referred to as the design frequency range), using an analysis frequency range of $f_{\mathrm{La}} = 2$ GHz to $f_{\mathrm{Ha}} = 10$ GHz. The antenna circumference C, defined by $C = 2\pi r_{\max}\ (= 2\pi \mathrm{a_{sp}}\phi_{\mathrm{end}})$, must be more than one wavelength at the lowest design frequency f_{Ld} [1], to support a traveling wave current necessary for CP radiation; C is chosen to be approximately 2 wavelengths at the lowest design frequency f_{Ld} in this paper. Based on this circumference, the diameter of the conducting cavity is chosen to be slightly larger than that of the spiral.

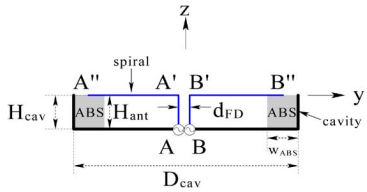

Fig. 2. Side view of a balanced-mode spiral (BALS).

In order to absorb the current reaching the outermost section of the arms, a ring-shaped strip absorber (ABS) of thickness w_{ABS} is placed inside the cavity. The absorber used in this paper is non-conducting TDK EM absorber (model ISFA), where the relative permittivity $\varepsilon_{\mathrm{r}}\ (= \varepsilon' - j\varepsilon'')$ and dielectric loss $(\tan\delta = \varepsilon''/\varepsilon')$ are frequency-dependent; ε' varies from $\varepsilon' = 2.00$ to 1.78 and $\tan\delta$ varies from 0.75 to 0.41 within the design frequency range of f_{Ld} (3 GHz) to f_{Hd} (9 GHz). Note that the radiation characteristics of the BALSs with and without this TDK absorber have already been discussed in [13].

The configuration parameters used in Section III are as follows: $D_{\mathrm{cav}} = 80$ mm for the cavity, $\mathrm{a_{sp}} = 1.273$ mm/rad, $\phi_{\mathrm{st}} = 0.5\pi$ rad, $\phi_{\mathrm{end}} = 8.5\pi$ rad, $w = 2$ mm, and $d_{\mathrm{FD}} = 1$ mm for the conducting strip arms, and $w_{\mathrm{ABS}} = 11$ mm for the absorber. In this case $D_{\mathrm{cav}}/2r_{\max} = 1.18$. The antenna height H_{ant} (= cavity height H_{cav}) is fixed to be 7 mm. Note that supplemental data on the absorber thickness w_{ABS}, antenna height H_{ant}, and spacing between the vertical conducting strip arms d_{FD} are presented in Section IV.

III. Analysis Results and Discussion

The antenna height/cavity is chosen to be less than half the wavelength at the highest design frequency f_{Hd} (9 GHz), thereby avoiding a dip in the radiation around the z-axis (note: the dip is caused by the radiation reflected from the bottom plane of the cavity). The antenna height in this section is $H_{\mathrm{ant}} = H_{\mathrm{cav}} = 7$ mm $= 0.21$ wavelength at f_{Hd}. Note that this antenna height is extremely small at low frequencies: 0.047 wavelength at the lowest analysis frequency f_{La} (2 GHz) and 0.07 wavelength at the lowest design frequency f_{Ld} (3 GHz).

A. Input Impedance and VSWR

The electric field $\mathbf{E}(\mathbf{r}, t)$ and magnetic field $\mathbf{H}(\mathbf{r}, t)$ within the analysis space are obtained using the finite-difference time-domain method (FDTDM) [11], [12], where $\mathbf{r}$ and t denote the position vector and time, respectively. The current at the antenna input is calculated by integrating $F\mathbf{H}(\mathbf{r}, t)$ around the antenna input conductor, where F denotes the Fourier-transform operation. The input impedance $Z_{\mathrm{in}} = R_{\mathrm{in}} + jX_{\mathrm{in}}$ is calculated on the basis of this current. Fig. 3 shows the calculated input impedance of the UnBALS, together with the input impedance of the BALS, for comparison. These lead to the curves for the VSWR (relative to 50 ohms) shown in Fig. 4. It is found that the

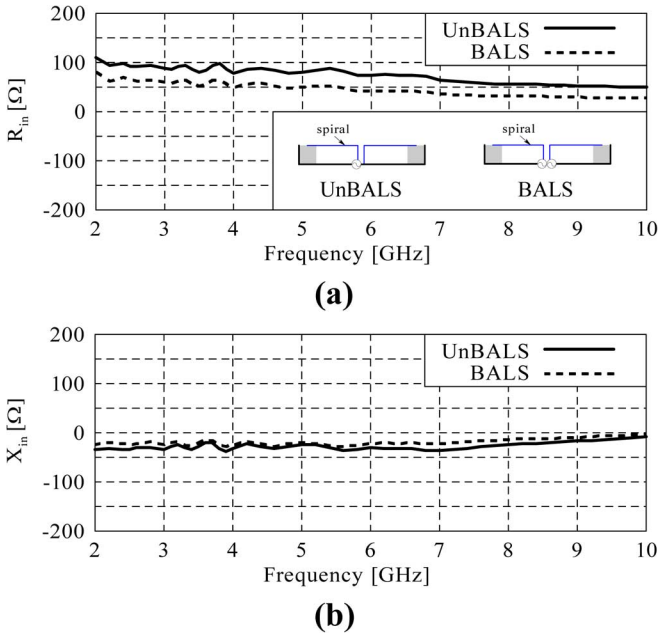

Fig. 3. Input impedances for UnBALS and BALS. (a) Input resistance $R_{\rm in}$ and (b) input reactance $X_{\rm in}$.

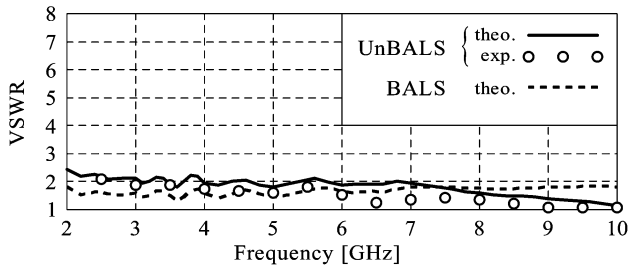

Fig. 4. VSWRs (relative to 50 ohms) for UnBALS and BALS.

VSWR for the UnBALS is acceptably small within the design frequency range of $f_{\rm Ld}$ (3 GHz) to $f_{\rm Hd}$ (9 GHz). For the most part, the VSWR is less than 2. The calculated results for the UnBALS are verified with experimental results (see the white dots).

B. Radiation Pattern and Current Distribution

The radiation field from the spiral, $\mathbf{E}_{\rm rad}$, is calculated on the basis of the equivalence principle [14], using the electric current $\mathbf{J}_e = \hat{n} \times F\mathbf{H}(\mathbf{r}, t)$ and magnetic current $\mathbf{J}_{\rm m} = F\mathbf{E}(\mathbf{r}, t) \times \hat{n}$ on a surface enclosing the spiral, where $\hat{n}$ is the outward unit vector normal to the surface. Fig. 5 shows the representative theoretical radiation patterns for the UnBALS at 3, 6, and 9 GHz, where the radiation field $\mathbf{E}_{\rm rad}$ is decomposed into a right-hand CP wave component $E_{\rm R}$ and a left-hand CP wave component $E_{\rm L}$. The radiation patterns for the BALS at the same frequencies are also presented in this figure. It is found that the UnBALS has a slightly asymmetric radiation pattern with respect to the z-axis, while the BALS has a consistently symmetric pattern. The asymmetry in the theoretical radiation pattern for the UnBALS, which is verified with experimental results (white and

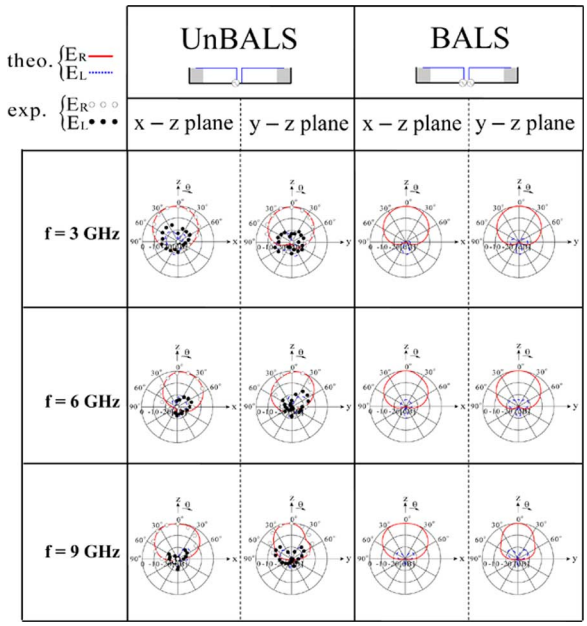

Fig. 5. Radiation patterns for UnBALS and BALS.

black dots in Fig. 5), can be explained by the behavior of the currents, as described in the following paragraphs.

Fig. 6 shows the currents of the UnBALS at 3, 6, and 9 GHz, where I_{ex} and I_{pr} designate the currents on the excited and parasitic arms, respectively. The real part, imaginary part, and absolute value for each of I_{ex} and I_{pr} are expressed by $I_{\rm r}$, $I_{\rm i}$, and $|I|$, respectively. We decompose the currents I_{ex} and I_{pr} into an odd-mode current I_o and an even-mode current I_e

$$I_{ex} = I_o + I_e \tag{1}$$

$$I_{pr} = -I_o + I_e. \tag{2}$$

From the above, I_o and I_e are given as $I_o = (I_{ex} - I_{pr})/2$ and $I_e = (I_{ex} + I_{pr})/2$. I_o and I_e are shown in Fig. 7, where $I_{\rm r}$ and $I_{\rm i}$ denote their real and imaginary parts, respectively. According to current-band theory [1], the odd-mode current I_o forms active regions (responsible for the strong radiation), which exist on the ring-shaped areas whose circumferences on the spiral plane are approximately $n_{\rm odd}\lambda_{\rm f}$, where $n_{\rm odd} = 1, 3, 5, \ldots$, and $\lambda_{\rm f}$ is the wavelength at frequency f. The black inverted triangles on the top horizontal axis for I_o show the locations where the circumference is $n_{\rm odd}\lambda_{\rm f}$. These active regions contribute to the radiation of an axial beam, whose maximum intensity is in the z-direction. Note that the radiation from current I_o is referred to as the *odd-mode* radiation, and the fields of the odd-mode radiation at symmetrically opposite points with respect to the z-axis are in-phase.

On the other hand, the even-mode current I_e also forms active regions, which exist on the ring-shaped areas whose circumferences on the spiral plane are approximately $n_{\rm even}\lambda_{\rm f}$, where $n_{\rm even} = 2, 4, 6, \ldots$; the black inverted triangles on the top horizontal axis for I_e show the locations where the circumference is $n_{\rm even}\lambda_{\rm f}$. These active regions contribute the radiation of a conical beam having zero-radiation in the z-direction and maximum radiation off the z-axis. The beam from this I_e is referred to as the *even-mode* radiation. Note that the fields

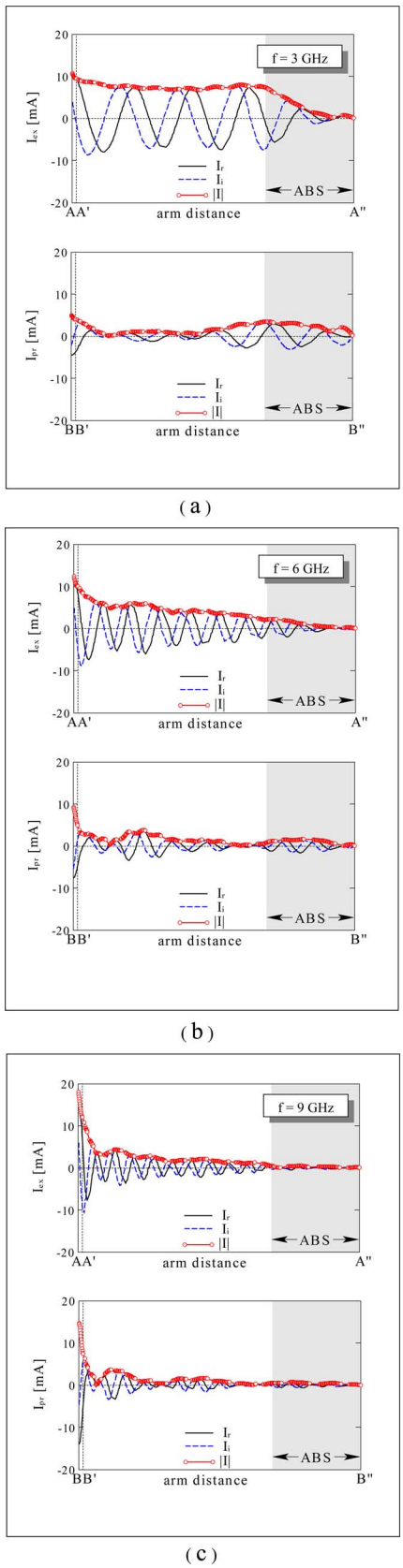

Fig. 6. Current distribution for UnBALS. (a) At 3 GHz, (b) at 6 GHz, and (c) at 9 GHz.

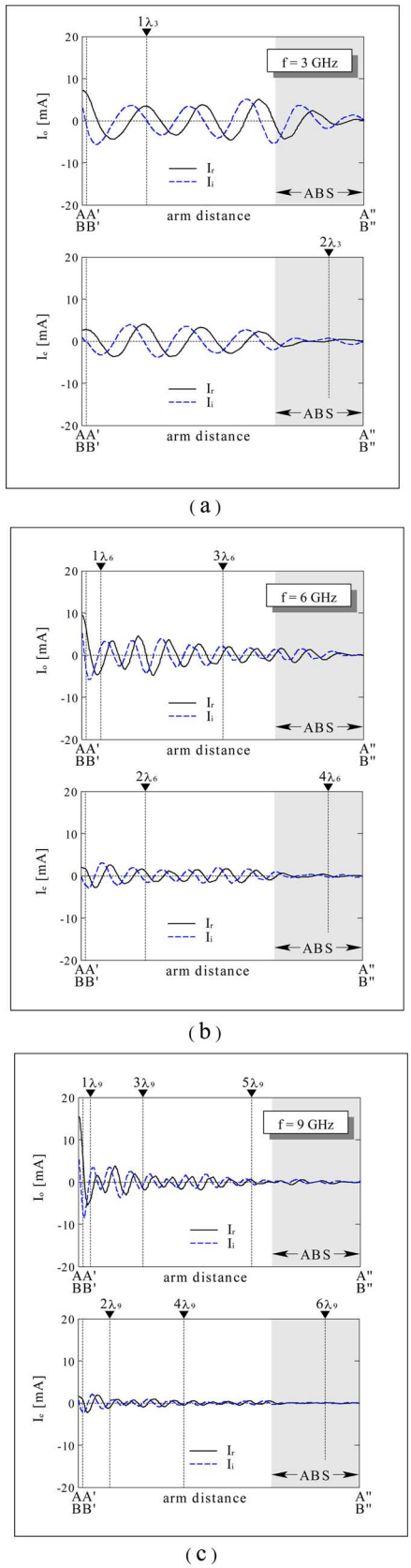

Fig. 7. Decomposition of the current for UnBALS. (a) At 3 GHz, (b) at 6 GHz, and (c) at 9 GHz.

of the even-mode radiation at symmetrically opposite points with respect to the z-axis are 180 degrees out of phase.

The total radiation is the sum of the odd-mode radiation and even-mode radiation. The even-mode radiation is constructively

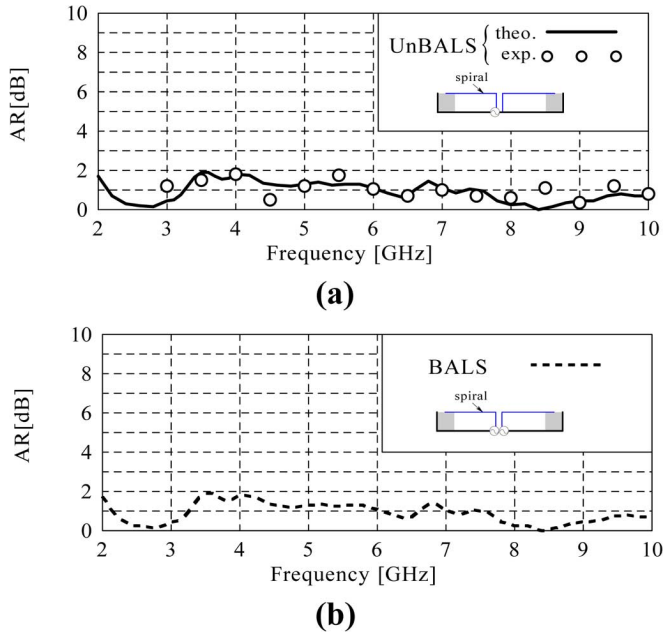

Fig. 8. Axial ratio (AR) as a function of frequency. (a) AR for UnBALS, where the solid curve shows theoretical results and the white dots show experimental results, and (b) AR for BALS.

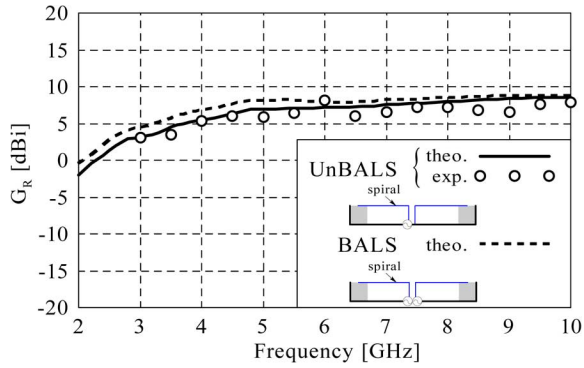

Fig. 9. Gains for UnBALS and BALS as a function of frequency.

and destructively superimposed on the odd-mode radiation, subject to the phase relationship between the two modes at symmetrically opposite points with respect to the z-axis. In other words, the odd- and even-mode radiation fields add positively on one side and add negatively on the other side. Thus, the radiation pattern of the axial beam from the odd-mode current, which is symmetric with respect to the z-axis, becomes asymmetric; that is, the beam direction deviates from the z-axis.

The azimuth angle $\phi_{\max}$ of the beam direction $(\theta_{\max}, \phi_{\max})$ varies with frequency [the zenith angle $\theta_{\max}$, measured from the z-axis, has a relatively small variation, which is not shown in this paper]. This means that the tilted beam rotates around the z-axis as the frequency changes. Consequently, the asymmetrical radiation pattern observed in a specific plane (for example, in the x-z plane or y-z plane) varies with frequency. Note that if $I_e = 0$, then the currents on the two arms are balanced with $(I_{ex}, I_{pr}) = (I_o, -I_o)$. In this case, no beam deviation occurs, as shown by the radiation pattern of the BALS in Fig. 5.

The circumference of the spiral in terms of the wavelength at 3 GHz is slightly larger than two wavelengths $(2\lambda_3)$. This antenna size supports the even-mode active region whose circumference is close to $2\lambda_3$. As seen from the bottom figure of Fig. 7(a), the amplitude of the even-mode current I_e on this active region at 3 GHz (the active region exists near the inverted triangle marking on the top horizontal axis) is very small, and hence the radiation field is dominated by odd-mode radiation, with a minimal effect from the even-mode radiation. It follows that the radiation pattern at 3 GHz becomes almost symmetric with respect to the z-axis, even though an even-mode current I_e exists.

The even-mode currents at 6 and 9 GHz are not small (relative to the odd-mode currents), as seen from the bottom figures of Fig. 7(b) and (c). At 6 GHz, the even-mode active region whose circumference is approximately $2\lambda_6$ shown in Fig. 7(b) affects the odd-mode radiation; similarly, at 9 GHz, the even-mode active regions whose circumferences are approximately $2\lambda_9$ and $4\lambda_9$ shown in Fig. 7(c) affect the odd-mode radiation. As a result, the radiation patterns at 6 and 9 GHz are asymmetric with respect to the z-axis, as seen from the radiation pattern in the UnBALS of Fig. 5. However, these asymmetries are not remarkable, and the UnBALS shows radiation patterns similar to those of the BALS.

C. Axial Ratio and Gain

After decomposing radiation field $\mathbf{E}_{\rm rad}$ into a right-hand CP wave component $E_{\rm R}$ and a left-hand CP wave component $E_{\rm L}$, the axial ratio (AR) is calculated. As observed in Fig. 5, the asymmetry of the radiation pattern with respect to the z-axis is not significant, and hence we infer that the axial ratio of the UnBALS in the z-direction normal to the antenna plane will be small over a wide frequency range, as desired. This is confirmed by the solid curve of Fig. 8(a), which shows the calculated AR results in the z-direction of the UnBALS as a function of frequency. For comparison, the axial ratio of the BALS is also presented in Fig. 8(b). It is revealed that the frequency response of the axial ratio of the UnBAL is similar to that of the BALS, showing small values of less than 3 dB (required for CP radiation) within the design frequency range (3–9 GHz). We can also see that the experimental results (white dots) in Fig. 8(a) are in good agreement with the theoretical results.

The radiation from the UnBALS at a point (r, θ, ϕ) within the positive z-space shown in Fig. 1 is circularly polarized (CP) with a right-hand sense. The right-hand CP gain relative to an isotropic antenna is given as $G_{\rm R} = G_{\rm a}/P_{\text{R-loss}}$, where $G_{\rm a} = (|E_{\rm R}|^2 + |E_{\rm L}|^2) r^2/30P_{\rm in}$ and $P_{\text{R-loss}} = 1 + \{(AR-1)/(\mathrm{AR}+1)\}^2$. Note that $G_{\rm a}$ is the absolute gain; $P_{\text{R-loss}}$ is the polarization loss; and $P_{\rm in}$ is the power observed at the antenna input, not including the loss due to impedance mismatching between the antenna and the feed line. Fig. 9 shows the gain $G_{\rm R}$ for the UnBALS, together with that for the BALS, both calculated in the z-direction $(\theta = 0)$. It is found that the gain $G_{\rm R}$ for the UnBALS is almost the same as that for the BALS. As the frequency increases, the gain approaches a value of approximately 8.5 dBi. The theoretical gain of the UnBALS is verified with experimental results (white dots).

From the analysis results in Sections III-A–C, it can be said that an UnBALS of height 7 mm has wideband CP antenna

characteristics comparable to those observed in a corresponding BALS, except for slight asymmetric radiation pattern. This UnBALS has the advantage over the BALS that it has a simple feed system (it does not need a balun circuit).

IV. Supplemental Data on Absorber Thickness w_{ABS}, Antenna Height H_{ant}, and Feed Line Spacing d_{FD}

A low-profile, wideband, circularly polarized UnBALS backed by a cavity is realized in Section III. This section presents supplemental data for gaining a better understanding of the UnBALS. The absorber thickness w_{ABS}, antenna height H_{ant}, and feed line spacing d_{FD} are discussed.

A. Absorber Thickness w_{ABS}

The thickness of the ring-shaped absorber is fixed to be $w_{\mathrm{ABS}} = 11\ \mathrm{mm}$ in Section III, where the inner radius of the absorber is 29 mm $\equiv r_{\mathrm{in}/0}$ (original inner radius) and the outer radius is $40\ \mathrm{mm} = D_{\mathrm{cav}}/2 \equiv r_{\mathrm{out}/0}$ (original outer radius) [note: $r_{\mathrm{out}/0} - r_{\mathrm{in}/0} = w_{\mathrm{ABS}}$].

If the outer radius of the ring-shaped absorber, r_{out}, is increased from the original value of $r_{\mathrm{out}/0} = 40\ \mathrm{mm} = D_{\mathrm{cav}}/2$, while holding the inner radius r_{in} at its original value of $r_{\mathrm{in}/0} = 29\ \mathrm{mm}$, the antenna characteristics, including the radiation efficiency, VSWR, radiation pattern, axial ratio, and gain, remain almost unchanged within the design frequency range of $f_{\mathrm{Ld}} = 3$ GHz to $f_{\mathrm{Hd}} = 9$ GHz. Noticeable improvement is not found with this thicker absorber at the lowest design frequency $f_{\mathrm{Ld}} = 3$ GHz.

It is also found that removing the vertical wall of the cavity (with a ring-shaped absorber of $r_{\mathrm{in}} = r_{\mathrm{in}/0}$ and $r_{\mathrm{out}} \geq r_{\mathrm{out}/0}$) does not deteriorate the antenna characteristics. It follows that the vertical wall of the cavity is not needed; it is used to stabilize the packaging of the spiral and absorber.

Further calculation is performed by varying the inner radius r_{in}. It is revealed that, as the inner radius r_{in} is decreased from the original inner radius of $r_{\mathrm{in}/0} = 29\ \mathrm{mm}$, while holding the outer radius at the original value of $r_{\mathrm{out}/0} = 40\ \mathrm{mm} = D_{\mathrm{cav}}/2$ [resulting in a thicker absorber], the radiation efficiency becomes smaller. For example, at middle design frequency $f_{\mathrm{Md}} = 6$ GHz, the radiation efficiency decreases from 78% (for the original inner radius $r_{\mathrm{in}/0} = 29\ \mathrm{mm}$) to 18% (for $r_{\mathrm{in}} = 1.5\ \mathrm{mm}$, where the absorber covers nearly the entire area behind the spiral, except for the feed area). This decrease in the radiation efficiency is due to the fact that the absorber is in contact with the two spiral arms and acts as a resistive load between the two arms. As the inner radius r_{in} is decreased (i.e., as the absorber thickness w_{ABS} is increased), there is greater contact between the two arms and the absorber, extending from the arm end area to the feed point area, causing the current traveling toward the arm ends to decay more rapidly. This results in a smaller radiation efficiency. If the absorber is not in contact with the spiral arms (i.e., the distance from the bottom of the cavity to the top of the absorber, designated as the absorber height H_{ABS}, is smaller than the antenna height H_{ant}), then the radiation efficiency improves. For example, the radiation efficiency at f_{Md} is approximately 50% when the top surface of the absorber with $r_{\mathrm{in}} = 1.5\ \mathrm{mm}$ is 2.5 mm ($H_{\mathrm{ant}} - H_{\mathrm{ABS}} = 7\ \mathrm{mm} - 4.5\ \mathrm{mm}$) away from the spiral arms. However, the VSWR and axial ratio deteriorate at lower frequencies, because the current reflected from the arm ends is no longer absorbed by the absorber, which is not in contact with spiral arms.

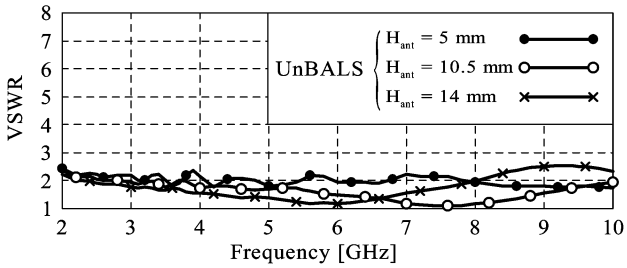

Fig. 10. VSWR (relative to 50 ohms) for UnBALS with the antenna height H_{ant} as a parameter.

B. Antenna Height H_{ant}

The antenna height $H_{\mathrm{ant}} (= H_{\mathrm{cav}})$ in Section III is fixed to be 7 mm ($\equiv H_{\mathrm{ant}/0}$: original antenna height). In this subsection, we investigate the effect of the antenna height on the antenna characteristics. For this purpose, we use three values of antenna height near the original value $H_{\mathrm{ant}/0}$: $H_{\mathrm{ant}} = 5\ \mathrm{mm}$, 10.5 mm, and 14.0 mm. These values are still less than half the wavelength at the highest design frequency f_{Hd} (9 GHz). Note that a height of $H_{\mathrm{ant}} = 16.7\ \mathrm{mm}$ corresponds to half the wavelength at f_{Hd}.

Figs. 10–13 show the VSWR, radiation pattern, axial ratio, and gain as a function of the frequency, with the antenna height as a parameter. It is found that the UnBALS exhibits a small VSWR (of less than 2.5, see Fig. 10). Each of the radiation patterns at the lowest design frequency ($f_{\mathrm{Ld}} = 3$ GHz) shows an almost symmetric pattern with respect to the z-axis, and it becomes asymmetric due to the effect of the even-mode radiation, as the frequency is increased (see Fig. 11). However, the axial ratio in the z-axis direction still remains small: less than 3 dB in the analysis frequency range of f_{La} (2 GHz) to f_{Ha} (10 GHz), as shown in Fig. 12.

As seen from Fig. 13, the gains for $H_{\mathrm{ant}} = 10.5\ \mathrm{mm}$ and 14.0 mm show almost the same tendency at lower frequencies (below 7 GHz). However, as the frequency is increased above 7 GHz, the gain for $H_{\mathrm{ant}} = 14\ \mathrm{mm}$ decreases. This is attributed to the phase difference between the primary radiation (which directly radiates from the spiral plane into free space) and the secondary radiation (which travels first toward the cavity from the spiral plane, is then reflected at the bottom of the cavity, and finally radiates into free space). As the frequency is increased, the antenna height in terms of wavelength approaches half the wavelength and the secondary radiation is superimposed negatively on the primary radiation. Consequently, the radiation in the z-direction has a dip, resulting in a reduction in the gain.

Comparisons of the antenna characteristics (VSWR, radiation pattern, axial ratio, and gain) for $H_{\mathrm{ant}} = 10.5\ \mathrm{mm}$ with those for the original height $H_{\mathrm{ant}/0} = 7\ \mathrm{mm}$ discussed in Section III reveal that the characteristics for the two cases are similar to each other within the design frequency range of f_{Ld} to f_{Hd}. It is also observed that the gain for $H_{\mathrm{ant}} = 5\ \mathrm{mm}$ is lower than that for $H_{\mathrm{ant}/0} = 7\ \mathrm{mm}$ at most frequencies within the design frequency range of f_{Ld} to f_{Hd} (see Figs. 9

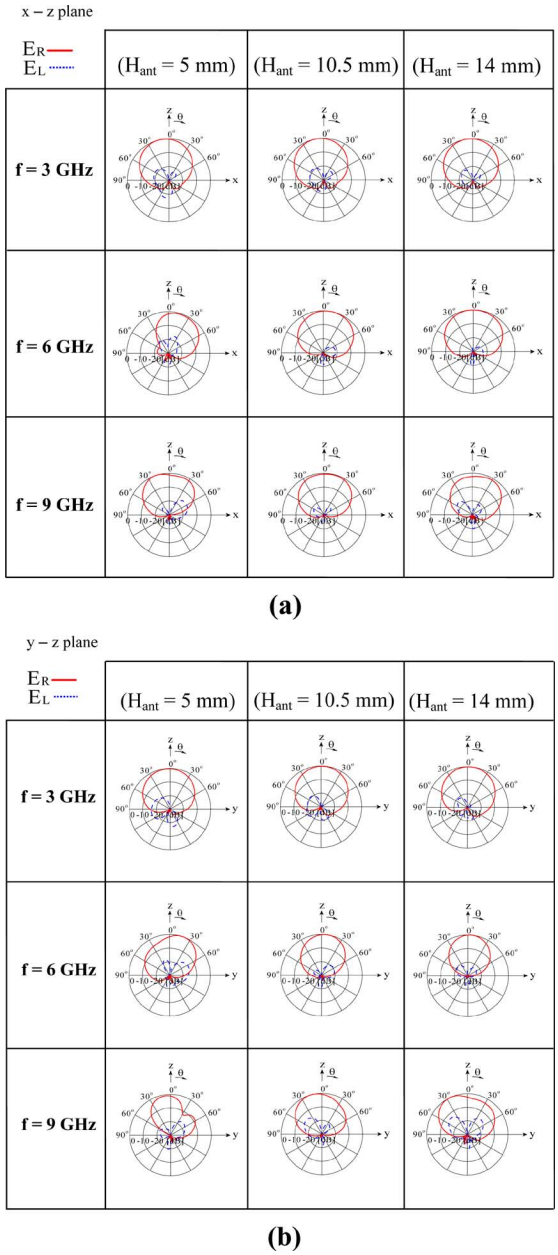

Fig. 11. Radiation pattern for UnBALS with the antenna height $H_{\rm ant}$ as a parameter. (a) In the x-z plane and (b) y-z plane.

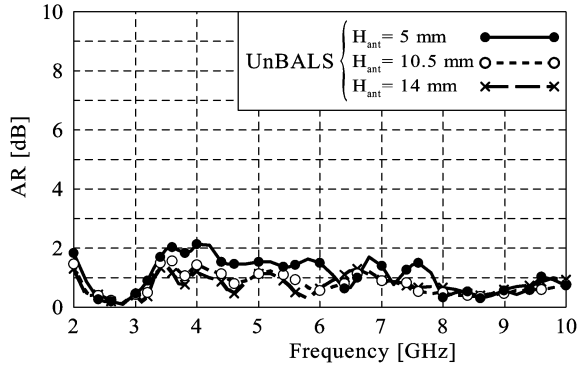

Fig. 12. Axial ratio (AR) for UnBALS with the antenna height $H_{\rm ant}$ as a parameter.

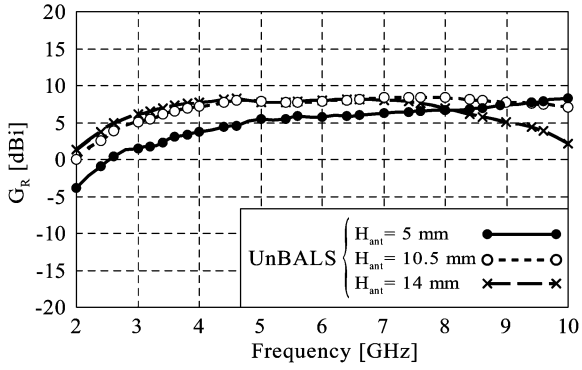

Fig. 13. Gain for UnBALS with the antenna height $H_{\rm ant}$ as a parameter.

and 13). From these comparisons of the antenna characteristics for $H_{\rm ant} = 10.5$ mm, $H_{\rm ant/0} = 7$ mm, and $H_{\rm ant} = 5$ mm, it can be said that choosing the antenna height to be the original height $H_{\rm ant/0} = 7$ mm is acceptable for realizing a low-profile CP spiral antenna.

C. Feed Line Spacing $d_{\rm FD}$

A planar spiral antenna, characterized by an Archimedean function and isolated in free space, has wideband characteristics with respect to the input impedance, radiation pattern, and gain, when the *strip* arm width w and the spacing between neighboring arms, w^*, are chosen to be the same: $w = w^*$ [13]. Using the spiral constant $a_{\rm sp} = 1.273$ mm/rad [which defines the centerline of the spiral strip arm] described in Section II results in a spiral that satisfies the $w = w^*$ condition when $w = 2$ mm (this spiral constant is used throughout the paper). From this fact, one would expect the antenna to have wideband characteristics, although the spiral in this paper is not purely isolated in free space (backed by a cavity). Note that this strip arm is approximated using staircases for the FDTDM calculation, where the length of a staircase [cell size for the FDTDM] is chosen to be $\Delta x = \Delta y = \Delta z = 0.5$ mm.

The spacing between the two vertical strip arms is fixed to be $d_{\rm FD} = 1$ mm $\equiv d_{\rm FD/0}$ in Section III. Additional analysis is performed using $d_{\rm FD} = 0.5$ mm and 1.5 mm. It is found that the radiation pattern, axial ratio, and directivity obtained for the original $d_{\rm FD/0}$ remain almost unchanged for the two additional variations of $d_{\rm FD}$. However, the input impedances are different from that for the original $d_{\rm FD/0} = 1$ mm, as shown in Fig. 14, where the input impedance for $d_{\rm FD/0}$ (UnBALS in Fig. 3) is also shown, for easy comparison. It is found that, as $d_{\rm FD}$ is increased, the input resistance $R_{\rm in}$ increases, with a small variation in the reactance $X_{\rm in}$. This fact is used for achieving an impedance match between the UnBALS and the feed line. Choosing $d_{\rm FD} = 1$ mm is acceptable for a 50-ohm feed line over the design frequency range of $f_{\rm Ld} = 3$ GHz to $f_{\rm Hd} = 9$ GHz (see Fig. 4).

V. Conclusion

A two-arm unbalanced-mode spiral (UnBALS) is investigated over a frequency range from 3 GHz ($= f_{\rm Ld}$) to 9 GHz ($= f_{\rm Hd}$). One of the two arms of the UnBALS is fed by a coaxial line, with the other arm acting as a parasitic element. It is emphasized that the UnBALS does not have a balun circuit,

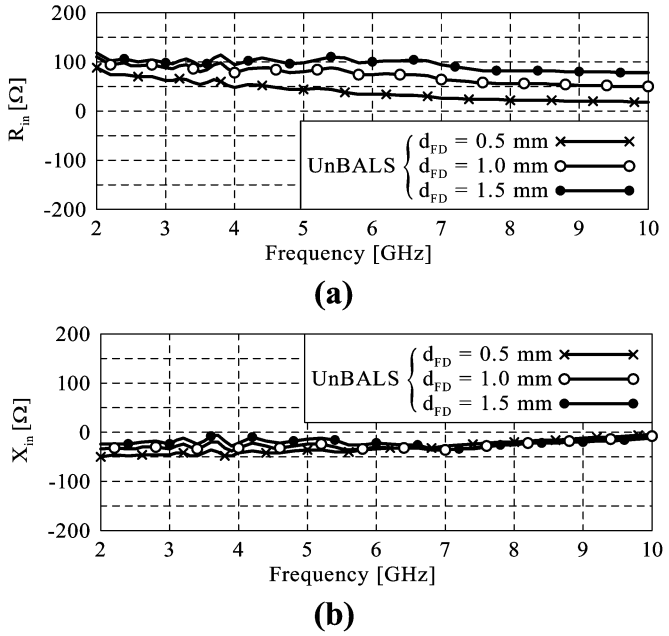

Fig. 14. Input impedance with the feed line spacing d_{FD} as a parameter. (a) Input resistance. (b) Input reactance.

which is required for a conventional two-arm balanced-mode spiral (BALS). The antenna characteristics for the UnBALS are compared with those for the BALS.

First, a small antenna height of 7 mm, corresponding to 0.07 wavelength at f_{Ld}, is used. The investigation reveals that the VSWR for the UnBALS is acceptably small within the frequency range of f_{Ld} to f_{Hd}, resulting in good input matching between the UnBALS and the feed line. The radiation pattern is slightly asymmetric with respect to the antenna axis (z-axis). This slight asymmetry is caused by the even-mode currents distributed on the two spiral arms. The analysis shows that the effect of the even-mode currents on the axial ratio near the antenna axis (z-axis) is small. The frequency response of the axial ratio in the z-direction is very similar to that for the BALS, showing values of less than 3 dB over a 100% design frequency range of f_{Ld} to f_{Hd}. The frequency response of the gain for the UnBALS is also similar to that for the BALS.

Second, for a better understanding of the UnBALS, the effects on the radiation characteristics of the absorber thickness w_{ABS}, antenna height H_{ant}, and feed line spacing d_{FD} are also discussed. As a result, the structure used in Section III is acceptable for realizing a low-profile, wideband, CP antenna that has a simple feed structure without a balun circuit.

ACKNOWLEDGMENT

The authors thank V. Shkawrytko and H. Mimaki for their assistance in the preparation of this manuscript.

REFERENCES

[1] J. A. Kaiser, "The Archimedean two-wire spiral antenna," *IRE Trans. Antennas and Propagation*, vol. AP-8, no. 3, pp. 312–323, May 1960.
[2] H. Nakano and J. Yamauchi, "A theoretical investigation of the two-wire round spiral antenna," in *Proc. IEEE Int. Symp. on Antennas and Propag.*, Seattle, WA, Jun. 1979, pp. 387–390.
[3] H. Nakano, *Helical and Spiral Antennas*. New York: Research Studies Press, 1987.
[4] H. Nakano, H. Yasui, and J. Yamauchi, "Numerical analysis of two-arm spiral antennas printed on a finite-size dielectric substrate," *IEEE Trans. Antennas Propag.*, vol. 50, no. 3, pp. 362–370, Mar. 2002.
[5] R. Bawer and J. J. Wolfe, "A printed circuit balun for use with spiral antennas," *IEEE Trans. MTT*, vol. 8, no. 3, pp. 319–325, May 1960.
[6] W.-H. Tu and K. Chang, "Wide-band microstrip-to-coplanar stripline/slotline transitions," *IEEE Trans. MTT*, vol. 54, no. 3, pp. 1084–1089, Mar. 2006.
[7] K. Hirose, M. Miyamoto, and H. Nakano, "A two-wire spiral antenna backed by a plane reflector with an unbalanced feed system," *IEICE Trans, Jpn.*, vol. J85-B, no. 4, pp. 520–528, Apr. 2002.
[8] J. J. H. Wang and V. K. Tripp, "Design of multioctave spiral-mode microstrip antennas," *IEEE Trans. Antennas Propag.*, vol. 39, no. 3, pp. 332–335, Mar. 1991.
[9] J. J. H. Wang, "The spiral as a traveling wave structure for broadband antenna applications," *Electromagnetics*, vol. 20, no. 4, pp. 323–342, Jul. 2000.
[10] H. Nakano, K. Kikkawa, Y. Iitsuka, and J. Yamauchi, "Equiangular spiral antenna backed by a shallow cavity with absorbing strips," *IEEE Trans. Antennas Propag.*, vol. 56, no. 8, pp. 2742–2747, Aug. 2008.
[11] K. S. Yee, "Numerical solution of initial boundary value problems involving Maxwell's equations in isotropic media," *IEEE Trans. Antennas and Propagation*, vol. AP-14, pp. 302–307, May 1966.
[12] A. Taflove, *Computational Electrodynamics: The Finite-Difference Time Domain Method*. Norwood, MA: Artech House, 1995.
[13] H. Nakano, S. Sasaki, H. Oyanagi, and J. Yamauchi, "Cavity-backed Archimedean spiral antenna with strip absorber," *IET Proc. Microw., Antennas Propag.*, vol. 2, no. 7, pp. 725–730, Oct. 2008.
[14] C. A. Balanis, *Antenna Theory: Analysis and Design*, 2nd ed. New York: Wiley, 1982, pp. 575–594.

Hisamatsu Nakano (M'75–SM'87–F'92) received the B.E., M.E., and Dr.E. degrees in electrical engineering from Hosei University, Tokyo, Japan, in 1968, 1970, and 1974, respectively.

Since 1973, he has been a member of the faculty of Hosei University, where he is now a Professor of electronic informatics. His research topics include numerical methods for low- and high-frequency antennas and optical waveguides.

Prof. Nakano received the IEE International Conference on Antennas and Propagation Best Paper Award and the IEEE TRANSACTIONS ON ANTENNAS AND PROPAGATION Best Application Paper Award (H. A. Wheeler Award) in 1989 and 1994, respectively. In 1992, he was elected an IEEE fellow for contributions to the design of spiral and helical antennas. He was also the recipient of the Chen-To Tai Distinguished Educator Award (from the IEEE Antennas and Propagation Society) in 2006. He is an Associate eDITOR of several journals and magazines, such as *IEEE Antennas and Propagation Magazine*, IEEE ANTENNAS AND WIRELESS PROPAGATION LETTERS and *Electromagnetics*.

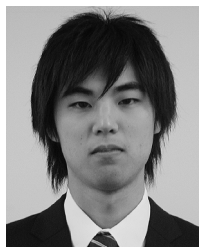

Tatsuya Igarashi was born in Tokyo, Japan, on October 11, 1985. He received the B.E. degree in electronic informatics from Hosei University, Tokyo, Japan, in 2008, where he is currently working toward the M.E. degree.

Mr. Igarashi is a Member of the Institute of Electronics, Information and Communication Engineers (IEICE) of Japan.

Hiroshi Oyanagi was born in Niigata, Japan, on September 22, 1986. He is currently working toward the B.E. degree in electronic informatics from Hosei University, Tokyo, Japan.

Mr. Oyanagi is a Member of the Institute of Electronics, Information and Communication Engineers (IEICE) of Japan.

Yasushi Iitsuka (M'98) was born in Ibaraki, Japan, on July 16, 1968. He received the B.E. degree in communication engineering and the M.E. degree in electrical engineering from Tokai University, Kanagawa, Japan, in 1992 and 1994, respectively. He is currently working toward the Ph.D. degree at Hosei University, Tokyo, Japan.

From 1994 to 2004, he was with Antenna Giken Co., Ltd., Saitama, Japan and from 2004 to 2006, was with Samsung Electro-Mechanics Co., Ltd., Suwon, South Korea. His current research interests are the design and analysis of antenna for mobile and satellite communication system.

Mr. Iitsuka is a member of the Institute of Electronics, Information, and Communication Engineers (IEICE) of Japan.

Junji Yamauchi (M'85–SM'08) was born in Nagoya, Japan, on August 23, 1953. He received the B.E., M.E., and Dr.E. degrees from Hosei University, Tokyo, Japan, in 1976, 1978, and 1982, respectively.

From 1984 to 1988, he served as a Lecturer in the Electrical Engineering Department, Tokyo Metropolitan Technical College. Since 1988, he has been a member of the faculty of Hosei University, where he is now a Professor. His research interests include optical waveguides and circularly polarized antennas. He is the author of *Propagating Beam Analysis of Optical Waveguides* (Research Studies Press, 2003).

Dr. Yamauchi is a member of the Optical Society of America and the Institute of Electronics, Information and Communication Engineers of Japan.